Nano Research 2015, 8(8): 2721–2732
DOI 10.1007/s12274-015-0779-x
Research Article
ISSN 1998-0124
CN 11-5974/O4

True-color real-time imaging and spectroscopy of carbon nanotubes on substrates using enhanced Rayleigh scattering

Wenyun Wu[1,§], Jingying Yue[1,§], Xiaoyang Lin[1,§], Dongqi Li[1,§], Fangqiang Zhu[2], Xue Yin[3], Jun Zhu[3], Jiangtao Wang[1], Jin Zhang[1], Yuan Chen[1], Xinhe Wang[1], Tianyi Li[1], Yujun He[1], Xingcan Dai[1] (✉), Peng Liu[1], Yang Wei[1], Jiaping Wang[1,4], Wei Zhang[5], Yidong Huang[5], Li Fan[1], Lina Zhang[1], Qunqing Li[1,4], Shoushan Fan[1], and Kaili Jiang[1,4] (✉)

[1] *State Key Laboratory of Low-Dimensional Quantum Physics, Department of Physics & Tsinghua–Foxconn Nanotechnology Research Center, Tsinghua University, Beijing 100084, China*
[2] *Department of Physics, Indiana University-Purdue University Indianapolis, Indianapolis, Indiana, USA*
[3] *State Key Laboratory of Precision Measurement Technology and Instruments, Department of Precision Instruments, Tsinghua University, Beijing 100084, China*
[4] *Collaborative Innovation Center of Quantum Matter, Beijing 100084, China*
[5] *Tsinghua National Laboratory for Information Science and Technology, Department of Electronic Engineering, Tsinghua University, Beijing 100084, China*
[§] *These authors contributed equally to this work.*

Received: 14 February 2015
Revised: 27 March 2015
Accepted: 2 April 2015

KEYWORDS
enhanced Rayleigh scattering,
Rayleigh imaging microscopy,
true-color imaging,
carbon nanotube,
interface dipole

ABSTRACT

Single-walled carbon nanotubes (SWCNTs) illuminated by white light should appear colored due to resonance Rayleigh scattering. However, true-color imaging of SWCNTs on substrates has not been reported, because of the extremely low scattering intensity of SWCNTs and the strong substrate scattering. Here we show that Rayleigh scattering can be greatly enhanced by the interface dipole enhancement effect. Consequently colorful SWCNTs on substrates can be directly imaged under an optical microscope by wide field supercontinuum laser illumination, which facilitates high throughput chirality assignment of individual SWCNTs. This approach, termed "Rayleigh imaging microscopy", is not restricted to SWCNTs, but widely applicable to a variety of nanomaterials, which enables the colorful nanoworld to be explored under optical microscopes.

Address correspondence to Xingcan Dai, XingcanDai@tsinghua.edu.cn; Kaili Jiang, JiangKL@tsinghua.edu.cn.

1 Introduction

The world we live in is colorful. An object is colored because it reflects or scatters some color component more than the others when illuminated by white light. The blue sky is the result of elastic scattering of sunlight by density fluctuations of air, which is well known as Rayleigh scattering [1]. Rayleigh scattering is also important in the nanoworld. In 2001, using a tungsten lamp as the white light source, Yu and Brus measured the Rayleigh scattering spectra of single-walled carbon nanotube (SWCNT) bundles, and observed resonance peaks due to the optically allowed interband transitions in SWCNTs [2]. Three years later, a supercontinuum (SC) white laser was employed to illuminate individual SWCNTs, which generated more distinct resonance Rayleigh scattering peaks [3]. Though excitonic in nature [4–7], the resonance peaks are related to the van Hove singularities (vHs) in the electron density of states, thus enabling chirality assignment of SWCNTs [8]. These resonance Rayleigh scattering peaks in the visible region imply that the SWCNTs should appear colored. Considering the fact that vHs are widespread in the electron density of states of 1-D nanomaterials, the nanoworld illuminated by white light should also be colorful. The displayed color information directly reflects the structures and physical properties of nanomaterials.

The question naturally arises whether nanomaterials are visible under an optical microscope so that people can peer into the colorful nanoworld? Unfortunately most nanomaterials, such as SWCNTs, are invisible under an ordinary optical microscope because of the extremely small Rayleigh scattering cross-sections of nanomaterials and the low intensity of excitation light. A general approach to this problem is to decorate the nanomaterials with some micrometer sized particles serving as scattering centers, such as solid micro-particles [9–11] or water microdroplets [12]. Another approach is to use fluorescence microscopy, which enables imaging of bio-nanomaterials functionalized by fluorescence proteins under an optical microscope with laser illumination [13–15]. Now the question becomes whether nanomaterials without functionalization can be directly imaged under an optical microscope simply by utilizing Rayleigh scattering. This question defines a research direction—imaging via Rayleigh scattering under an optical microscope, which we would like to term "Rayleigh imaging microscopy".

The ultimate goal of Rayleigh imaging microscopy is to achieve real-time true-color imaging of nanomaterials with super-resolution, similar to the relatively mature field of super-resolved fluorescence imaging microscopy. Several approaches have been developed to achieve this goal. The first key step is to utilize a SC white laser to increase the intensity of the excitation light [3], since the scattered light intensity is proportional to the intensity of the excitation light. This method is quite effective for suspended SWCNTs. However, for nanomaterials on substrates, severe scattering from the substrate reduces the contrast and thus hinders Rayleigh imaging. Therefore the second key step is to diminish the substrate scattering. Two methods have been employed. The first one is to immerse nanomaterials into a medium with a matching refractive index in order to eliminate the substrate scattering. In 2010, Joh and colleagues utilized quasi-monochromatic light filtered from a SC white laser by an acousto–optical tunable filter (AOTF) to illuminate SWCNTs on quartz substrates immersed in glycerol, and collected the scattered light using a highly sensitive CCD camera [6, 16]. By tuning the wavelength of the incident light, a series of images were recorded to reconstruct a false color Rayleigh image. The importance of their work is to demonstrate that Rayleigh imaging is viable. However, it is not real-time imaging. The second method to diminish the substrate scattering is using two Glan–Thomson polarizers to construct a home-built polarized light microscope [7, 17]. By using this method in 2011, Lefebvre and Finnie achieved Rayleigh imaging of suspended SWCNTs under the illumination of a tunable Ti-sapphire laser [17]. In 2013, by using the similar method but with a SC white laser as illumination source, Liu and colleagues achieved Rayleigh imaging of SWCNTs transferred onto a substrate [7]. Both groups demonstrate real-time Rayleigh imaging of SWCNTs under an optical microscope, but the images showed some special contrast and did not possess chirality-dependent color information. So far, although real-time Rayleigh imaging of SWCNTs has been demonstrated, true-color imaging of SWCNTs on a substrate has not been reported, and

super-resolution has not even been attempted.

Here we show that Rayleigh scattering can be greatly enhanced by the interface dipole enhancement effect. Consequently real-time true-color imaging of SWCNTs on substrates has been successfully achieved under an optical microscope by wide field SC laser illumination, which facilitates high throughput chirality assignment of individual SWCNTs.

2 Experimental

To achieve true-color real-time imaging of SWCNTs, we have developed Rayleigh imaging microscope which is composed of a standard optical microscope and a SC white laser as the oblique illuminating light source. Several setups of light illumination have been designed and tested to facilitate the Rayleigh imaging. The simple stand-alone SC white laser illumination setups make it easy to integrate with a spectrometer to construct the Rayleigh imaging assisted spectroscopy (RIAS) system, which combines real time imaging with *in situ* spectral measurements, and thus enables high throughput chirality assignment of SWCNTs.

2.1 Rayleigh imaging microscope

Figure 1(a) shows the schematic illustration of our experimental setup of a Rayleigh imaging microscope for true-color real-time imaging of nanomaterials. It simply comprises a SC white laser (Fianium SC400) as the oblique illuminating light source, and a standard optical microscope to collect the Rayleigh scattered light. The collimated output terminal of the SC laser can be inserted into one end of a home-made optical tube and a long working distance objective (M PLAN APO L 10X) is installed into the other end. Both are self-aligned to the tube axis. An edge filter (Semrock multiphoton filter 770/SP) was inserted between the output terminal and the objective to filter out the infrared light and avoid heating effects. A general purpose digital camera with a low cost CMOS image sensor (Canon EOS600D) was employed to conveniently record the images and real-time videos. Looking into the eyepiece is strictly prohibited in order to avoid any exposure of the eyes to the laser beam. In addition, an optical damper must be installed for safety reasons.

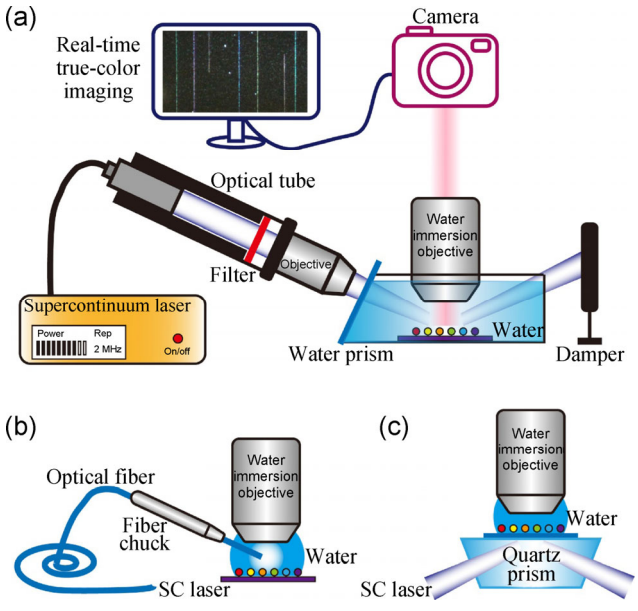

Figure 1 Schematic illustration of Rayleigh imaging microscope for true-color real-time imaging of SWCNTs on substrates. (a) Detailed structure of a Rayleigh imaging microscope by using an optical tube to filter out the infrared band and slightly focus the white laser beam on the samples through a water prism. (b) A single mode (850 nm) optical fiber is used instead of the water prism and the optical tube to filter out the infrared band and deliver the white laser beam to the samples. (c) Schematic illustration of the total internal reflection Rayleigh imaging microscope by using a quartz prism. The Rayleigh scattering of samples is excited by the evanescent wave.

The samples examined were horizontally aligned SWCNTs, which were first synthesized on quartz substrates by chemical vapor deposition (CVD) [18] and then transferred to Si wafers with 100 nm SiO_2 using poly(methyl methacrylate) (PMMA) [19]. To reduce substrate scattering, samples were immersed in water in a home-made water prism, which is a water container with a planar quartz window. The incident white laser beam (about 100 mW) was set vertical to the quartz window of the water prism to avoid dispersion, and focused into an area of approximately 100 μm × 100 μm by the long working distance objective. The scattered light was collected by a water immersion objective (Leica L 63X/0.9), which offers higher resolution than an ordinary lens used in air due to its higher numerical aperture.

A low cost setup was also designed and tested for the Rayleigh imaging microscopy (Fig. 1(b)). The SC laser we used is a NKT SuperK compact with 100 mW

power output, nanosecond pulse width, and a 25 kHz repetition rate. We connected one end of a single mode (850 nm) optical fiber to the photonic crystal fiber output via a FC/APC connector. The other end of the fiber was cut to obtain a fresh end face after the polymer coating was removed. This single mode fiber also serves as a filter to remove the infrared component of the white light. The total output power from the fresh end is only about 5 mW. The fresh end of the optical fiber was inserted into the droplet which was attached to the water immersion objective to illuminate the sample locally. When we moved the sample, the droplet slid on the surface because of the hydrophobic nature of the sample. This simple and low cost setup also enables real-time true-color Rayleigh imaging of nanomaterials.

Another setup was designed and tested for SWCNTs on a quartz substrate only, as shown in Fig. 1(c). A quartz prism was used to couple the SC white laser to illuminate the sample. The sample was adhered to the quartz prism by using a refractive index matching liquid (glycerol, n = 1.475). Similar to the setup shown in Fig. 1(b), a water droplet was attached to the water-immersed objective and slid freely on the surface of the sample. The incident beam was set normal to the side surface of the quartz prism. When it reached the top surfaces of the sample, the incident beam was totally internally reflected. The SWCNTs thus lie in the evanescent field at the interface between water and the quartz substrate. Rayleigh scattering is effectively excited by this evanescent wave. Similar to total internal reflection fluorescence (TIRF), this phenomenon should be called total internal reflection Rayleigh scattering.

2.2 True-color imaging of SWCNTs

Typical true-color images of horizontally aligned SWCNTs transferred onto a silicon substrate are shown in Figs. 2(a) and 2(b). As expected, the SWCNTs are colorful, indicating diverse chiral indices. The positions, lengths, densities, and morphologies of SWCNTs are also clearly displayed. The upper part of Fig. 2(b) shows random SWCNTs grown on the catalyst stripe. Only those SWCNTs parallel to the s-direction, i.e. perpendicular to the incident plane, can be seen,

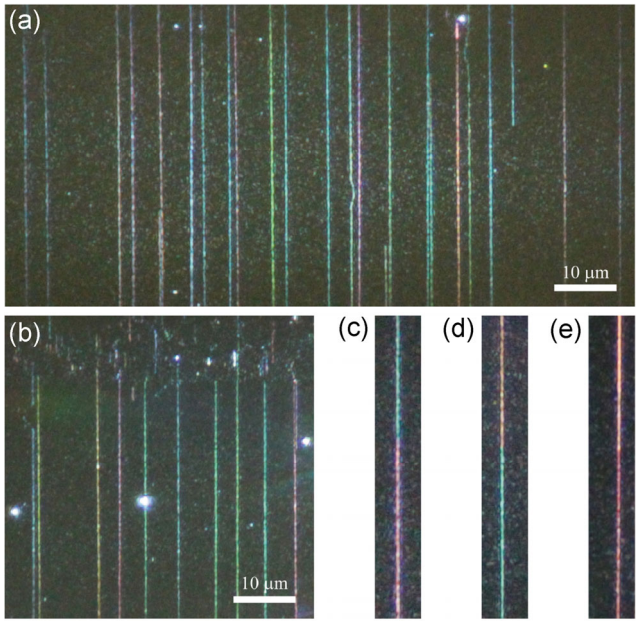

Figure 2 True-color imaging of SWCNTs. (a) Typical true-color image of horizontally aligned SWCNTs on a Si wafer with a layer of 100 nm SiO_2. (b) True-color image of horizontally aligned SWCNTs and some disordered SWCNTs on the catalyst stripe. (c)–(e) Typical true-color images of three individual SWCNTs with intramolecular junctions.

indicating the polarization effect of Rayleigh scattering. Furthermore, the abrupt color changes shown in Figs. 2(c)–2(e) clearly indicate the abrupt chirality changes within the individual SWCNTs, and therefore the true-color Rayleigh imaging technique provides a direct and efficient way for identifying intramolecular junctions. But for SWCNT bundles, double-walled carbon nanotubes (DWCNTs) or multi-walled carbon nanotubes (MWCNTs), the color is a mixture of colors from all the tubes, and individual tubes cannot be resolved due to the diffraction-limited imaging.

2.3 Rayleigh imaging assisted spectroscopy

The simple stand-alone SC white laser illumination setups can be easily integrated with other instruments. For example, they can be integrated with a spectrometer to construct a RIAS system, as shown in Fig. 3. In our experiment, RIAS is achieved simply by integrating a SC white laser illumination setup, as shown in Fig. 1(a), with a commercial micro-Raman system (Renishaw 2000 or HORIBA Jobin Yvon RM1000). The SC laser serves as the light source for both imaging and Rayleigh spectral measurement. Colorful SWCNTs are displayed

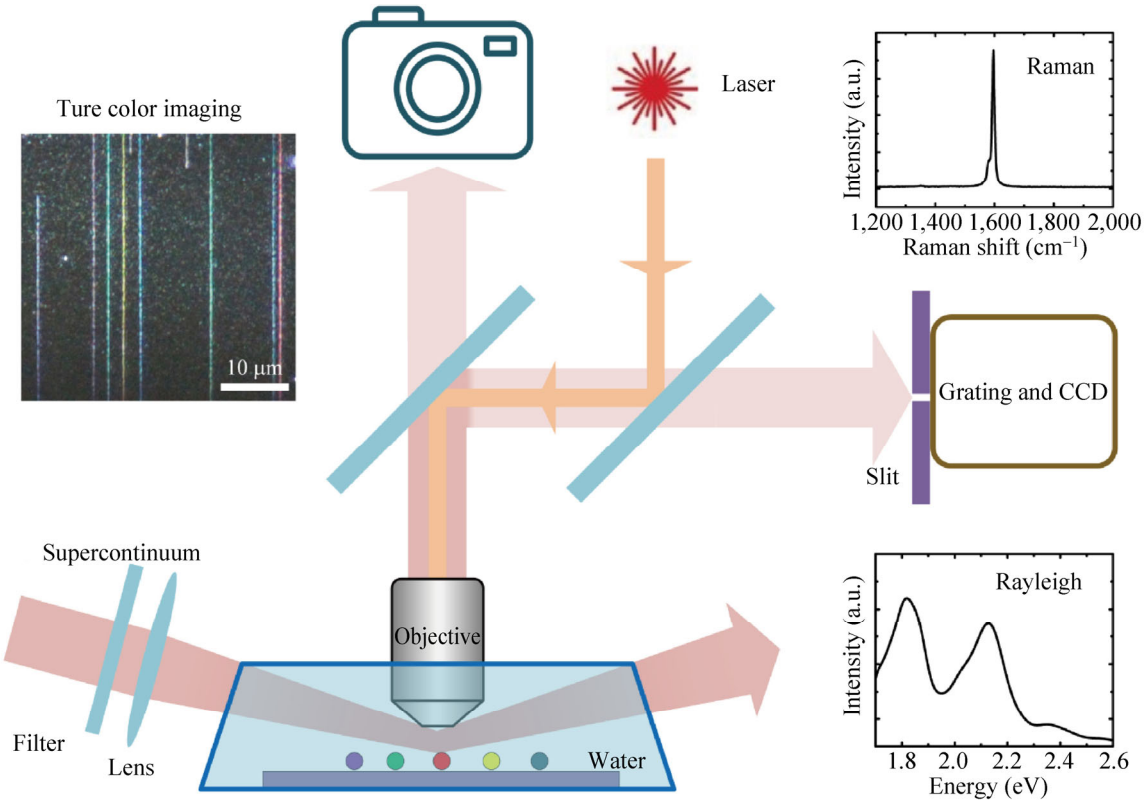

Figure 3 Schematic illustration of RIAS. Integration of Rayleigh imaging microscopy and optical spectroscopy for true-color real-time wide-field imaging and chirality assignment of SWCNTs.

in real-time on the screen which is connected to the digital camera (Canon EOS600D) and the true-color image can be captured. After individual SWCNTs are located, *in situ* Rayleigh and Raman spectra can be obtained alternately by switching the optical path and the light source. Elastic or inelastic scattered light is collected by an objective and then goes through a slit before being analyzed by a spectrometer. Our system combines real time imaging with *in situ* spectral measurements, and thus enables high throughput chirality assignment of SWCNTs.

2.3 Chirality assignment of SWCNTs by *in situ* optical spectroscopy

With the help of true-color real-time wide-field imaging, the targeted SWCNT can be easily and quickly located for subsequent Rayleigh and Raman spectral measurements, which enables high throughput chirality assignment. The true-color image of six SWCNTs in water is shown in Fig. 4(a), which provides additional color information compared with SEM image shown in Fig. 4(b). The Rayleigh spectra of all the six SWCNTs from left to right in order in Fig. 4(a) are displayed in Figs. 4(c)–4(f), respectively. The first, second, and sixth SWCNTs all have two resonant peaks in the visible region and the chiral indices are easily assigned. For the remaining three SWCNTs with a single resonant peak in the visible region (that is, 1.7–2.6 eV, according to the atlas we referred to, see Ref. [20]), additional diameter information provided by the radial breathing mode (RBM) in Raman spectra will greatly speed up the chirality assignment [21]. Traditionally it is time consuming to determine the required excitation wavelength (since resonant excitation is needed for RBM), but now with the help of the resonance information given by Rayleigh spectra, the required excitation wavelength can be easily selected. For example, the third and fifth nanotubes should be excited by a 633 nm laser and the fourth by a 514 nm laser. Combining Rayleigh and Raman spectra, the chiral indices of the six individual SWCNTs in Figs. 4(a) and 4(b) are assigned as (16, 12), (17, 12), (22, 3), (13, 9),

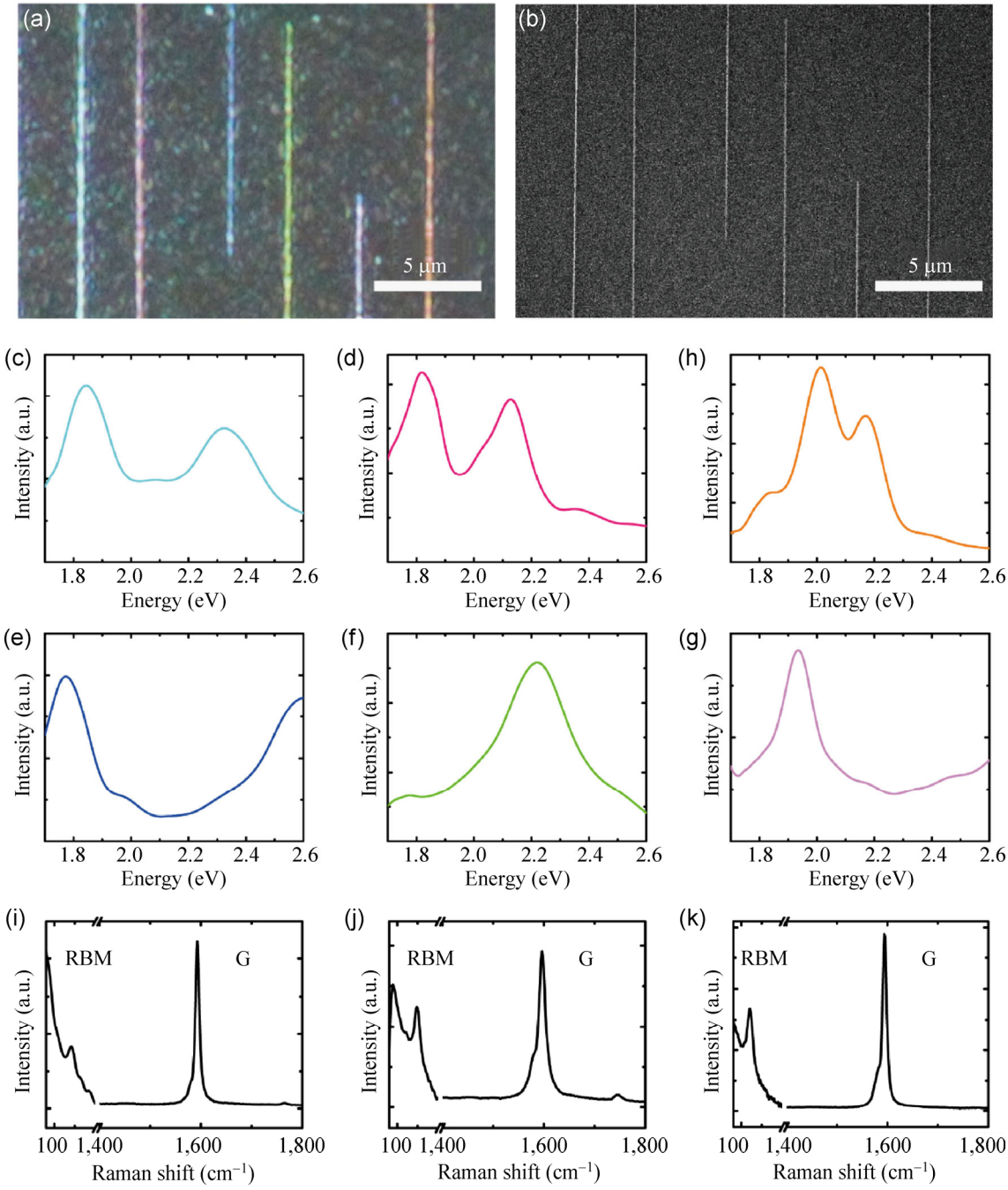

Figure 4 True-color imaging and spectroscopy of individual SWCNTs on a Si wafer. (a) True-color image of individual SWCNTs on a Si wafer with 100 nm SiO_2 immersed in water. (b) Corresponding SEM image of individual SWCNTs in (a). (c)–(h) Rayleigh spectra of all six individual nanotubes in (a) from left to right in order, whose chiral indices were identified as (16, 12), (17, 12), (22, 3), (13, 9), (17, 16), and (20, 6), respectively. (i)–(k) Raman spectra of the three SWCNTs whose Rayleigh spectra are shown in (e)–(g) respectively.

(17, 16), and (20, 6), respectively. Apparently, RIAS provides both high quality true-color imaging and high throughput chirality assignment of SWCNTs.

However, extreme caution should be exercised in chirality assignment of SWCNT bundles, DWCNTs or MWCNTs. In these cases, the strong tube–tube interactions might lead to a shift in peak positions compared to isolated SWCNTs [22, 23].

3 Results and discussion

So far, Rayleigh imaging microscopy and RIAS have been shown to work well for SWCNTs transferred from quartz substrates to Si wafers. A natural question is whether they work for as-grown SWCNTs on quartz substrates. Figure 5(a) shows the true-color image of SWCNTs on a quartz substrate in water, using the optical setup illustrated in Fig. 1(a). As expected, SWCNTs are colorful due to the resonance Rayleigh scattering. In contrast, the colors of SWCNTs in air (Fig. 5(b)) are less distinct, and many fewer SWCNTs are observed. Therefore, water must have played some important roles in improving the image quality.

We suggest that water has at least three effects on the Rayleigh imaging, namely refractive index matching, boundary field enhancement and interface dipole enhancement effects.

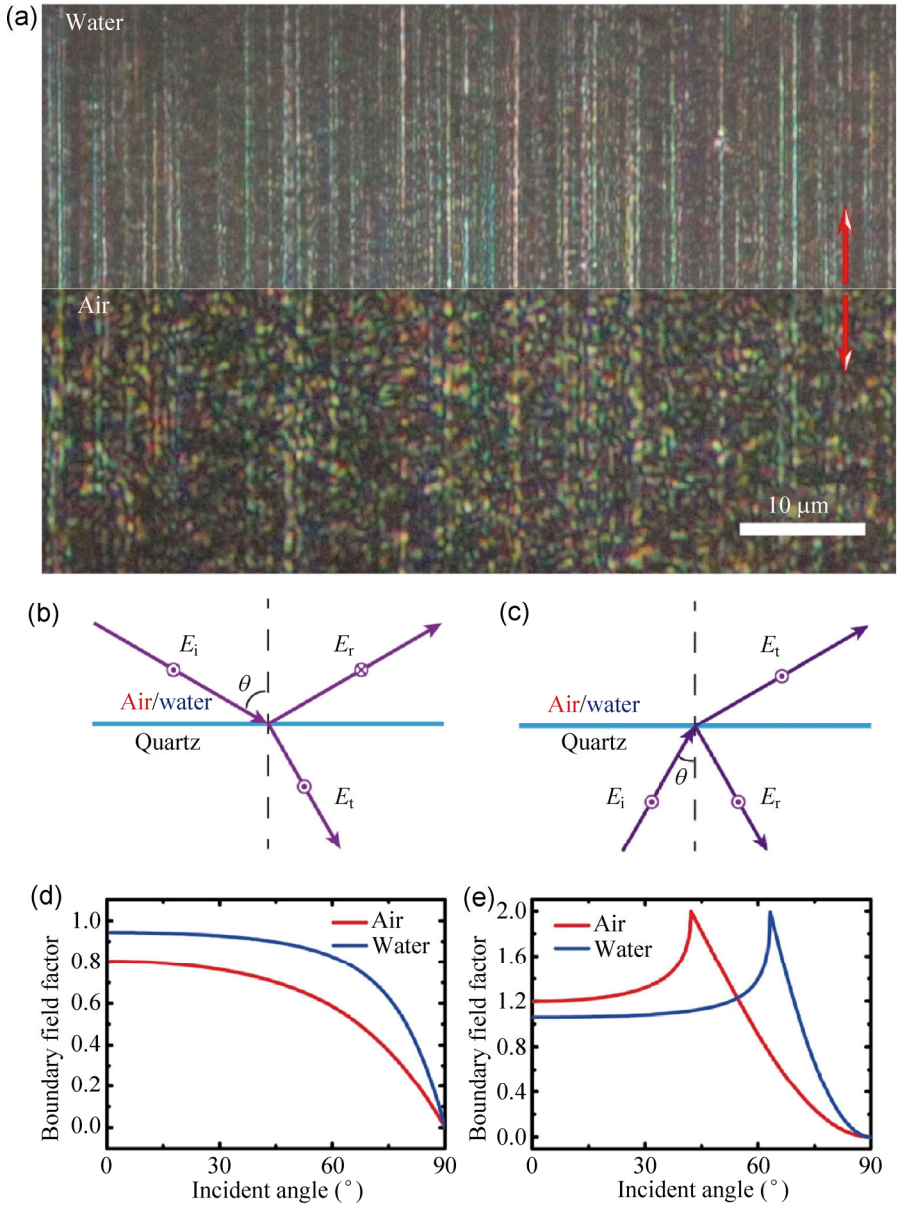

Figure 5 Rayleigh images of as-grown SWCNTs on quartz and the boundary field. (a) Rayleigh images of the same SWCNTs in water and in air, and the two images are mirror-symmetric with respect to the middle line. (b) and (c) Illustration of the reflection and refraction of the s-component of light at the air/quartz boundary or water/quartz boundary for the incident light lies in air/water (b) and in quartz (c). (d) and (e) The boundary field factors for the cases (b) and (c), respectively, when the incident field is s-polarized. The boundary field factor is defined as the ratio of the boundary field to that of the incident field.

3.1 Refractive index matching effect and boundary field enhancement effect

First, water serves as the refractive index matching medium, since the refractive index of water (n = 1.33) is close to that of quartz (n = 1.49). The index matching leads to greatly reduced scattering from the substrate, and therefore the contrast can be greatly improved. Second, the E-field at the water/substrate boundary (termed the "boundary field") is larger than that at the air/substrate boundary for the same intensity of incident light. Since we place the SWCNTs in the s-direction, and only the E-field polarized along the tube axis of the SWCNT will excite the Rayleigh scattering, only the s-component of the incident light needs to be considered in the following discussions. According to classical electrodynamics, a tangential E-field should be unchanged at two sides of the boundary. Therefore the s-wave boundary field is single-valued at both sides of the boundary. It can be calculated from either the transmitted E-field (or the evanescent E-field in the case of total internal reflection) or the summation of the incident and reflected E-fields shown in Figs. 5(b) and 5(c). We define the boundary field factor as the ratio of the amplitude of the boundary field to that of the incident field.

The calculated results are shown in Fig. 5(d) for the experimental setups shown in Figs. 1(a) and 1(b). In this case the incident beam lies in the optically less dense medium (water or air), hence the boundary field factors are always smaller than one, implying a weakened boundary field, because there is a π phase shift in the reflected E-field. At any incident angle less than 90°, the factor in water is always larger than that in air, indicating a boundary field enhancement when water is present.

For the experimental setup shown in Fig. 1(c), the incident beam lies in the optically dense medium (quartz). There is no phase shift when the incident angle is less than the critical angle, leading to boundary field factors larger than 1. As the incident angle increases from 0° to the critical angle, the reflectivity increases gradually to 1, resulting in the increase of the boundary field factor to its maximum value. When the incident angle increases from the critical angle to 90°, the reflectivity maintains a constant value of unity, but a phase shift occurs in the reflected E-field and it increases from 0 to π. As a result, the boundary field factor gradually decreases from its maximum to 0. In our experiments, we used an incident angle of 75°, and again the boundary field factor of water is larger than that of air, indicating an enhanced boundary field.

Here we would like to stress that boundary field enhancement alone cannot enhance the contrast for SWCNTs on a substrate, because the substrate scattering is simultaneously enhanced. For the different configurations in Figs. 1(a) and 1(c), the contrast of SWCNTs on a quartz substrate remains the same, although the scattering of SWCNTs in Fig. 1(c) can be greater (because of the larger boundary field) when the incident light intensity is the same. However, compared with air, water gives rise to both diminished substrate scattering and an enhanced boundary field, thus leading to much higher contrast Rayleigh images.

3.2 Interface dipole enhancement effect

If we can find a method to locally enhance the E-field acting on the SWCNTs rather than the whole substrate, then the contrast of the Rayleigh image will be further improved. Fortunately, a combination of experimental and theoretical investigations indicates that such an enhancement effect does exist, and we have previously described this as the "interface dipole enhancement effect" (IDEE) [24]. IDEE comes into play when a SWCNT is surrounded by a thin interfacial layer of high refractive index material provided that: (1) The interfacial layer of the high refractive index material must be thin enough to guarantee that the Rayleigh scattering from this layer is weaker than that from the nanomaterial; (2) for the high refractive index material, there are no characteristic Rayleigh scattering peaks from the interfacial molecules in the visible region. The interfacial layers we have tested and found to be effective include water, glycerol, Refractive Index (Matching) Liquids, cedar oil, isopropanol, and PMMA.

Considering that the diameter of a SWCNT is about 1 nm, the first prerequisite is that the thickness of the interfacial layer should be a few nanometers or less. According to classical electrodynamics simulations using the finite difference time domain (FDTD) method, which is based on the macroscopic field calculation,

the field enhancement by a nanometer thickness shell is negligible. However, the local field produced by the nanometer shell, which is a microscopic quantity and not accessible in macroscopic field calculations, might play an important role in the enhancement effect.

To calculate the local field, a microscopic picture must be adopted, in which the atoms, molecules or clusters surrounding the SWCNT are viewed as optical dipoles driven by the light field. Both the near field and the far field of the nanometer shell are easily obtained by summing up the field of these optical dipoles. Since the characteristic length of the local field region, the diameters of the SWCNTs, and the thickness of the high refractive index shell, are all much smaller than the wavelength of incident light, a static field approximation is justified in calculating the near field.

The calculation results indicate that there are indeed some local field enhanced regions which can lead to enhanced Rayleigh scattering. However, this local field decays very rapidly with increasing distance from the dipoles. Therefore this enhancement effect is an interface phenomenon, which is why we describe it as the "interface dipole enhancement effect". A detailed discussion of IDEE can be found in Ref. [24]. With the help of IDEE, the enhanced local field acting on SWCNTs can lead to interface dipole enhanced Rayleigh scattering which enables true-color real-time Rayleigh imaging.

Previous results [25, 26] and our molecular dynamics simulations (details can be found in Ref. [24]) indicate that, when a SWCNT is immersed in water, cylindrical shells of condensed water molecules will automatically form around the SWCNT. The density of water molecules in the first neighboring cylindrical shell is about 2.7 times that of the average level. According to the Clausius–Mossotti relation [27], an increase in number density of molecules always leads to an increase in dielectric constant as well as refractive index. Thus this sub-nanometer shell of high density water serves as the interfacial layer of a high refractive index material, which might lead to the interface dipole enhanced Rayleigh scattering.

Compared with the images of as-grown SWCNTs on quartz substrates, the images of PMMA-transferred SWCNTs on silicon wafers always show much better color contrast. Comparing the optical images with SEM images, we found that on quartz substrates there are always some SWCNTs invisible in the Rayleigh image. In contrast, those transferred onto Si wafers are all visible in the corresponding Rayleigh image. However, the boundary field calculations indicate that the quartz substrate and the silicon wafer have similar boundary field factors. The difference might originate from two factors: (1) The roughness of Si wafers is much smaller than that of quartz substrates, thus resulting in much lower substrate scattering; (2) the residual PMMA on SWCNTs leads to a larger enhancement effect than the high density water shell.

In the aforementioned two cases (as shown in Figs. 2 and 4(a)), it may be argued that the contrast enhancement is totally contributed by a refractive index matching effect without the help of IDEE. Here we provide decisive evidence for the existence of the IDEE. When the substrate was put in air, a severe substrate scattering occurred, and SWCNTs are very dim in Rayleigh image. Then we dropped a tiny droplet of glycerol onto the surface of the quartz, and took a series of images during the diffusion process. Three images are selected from the image series and shown in Figs. 6(a)–6(c). The boundary of the droplet can be clearly discerned, and appears unchanged. Between the droplet boundary and the catalyst stripe marked in Fig. 6(b), excess glycerol on the SWCNTs forms microspheres, which dominate the scattering, and so the SWCNTs do not show chirality-dependent colors. Below the catalyst stripe, the SWCNTs are covered by a wetting layer of glycerol, resulting in interface dipole enhanced Rayleigh scattering of the SWCNTs, showing their distinct chirality-dependent colors. The background is dark because the enhanced Rayleigh scattering from SWCNTs is very strong, so that we have to shorten the integration time for imaging. These results clearly prove the existence of IDEE. The full process can be observed in the supplementary video which is made up of the snapshots taken during the diffusion of glycerol along the SWCNTs.

Moreover, we believe that IDEE is significant and widespread for nanomaterials surrounded by condensed media. For example, solutions of single-chirality SWCNTs wrapped by surfactant molecules display chirality-dependent colors [28, 29] in which the IDEE

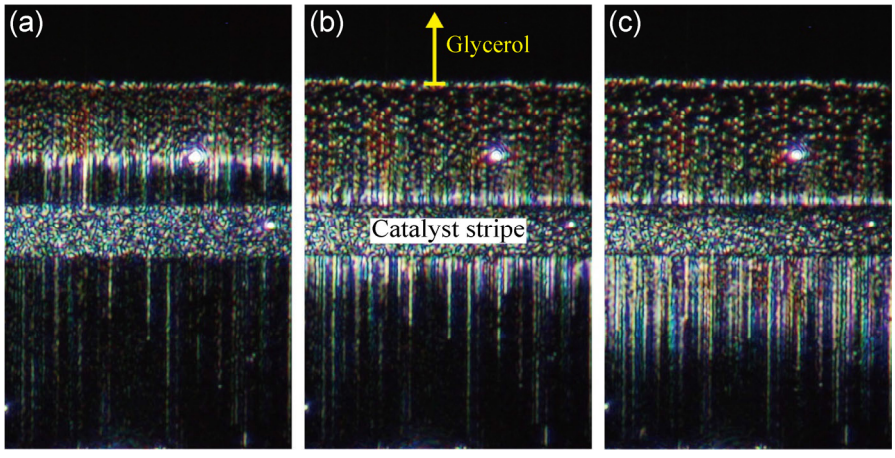

Figure 6 Interface dipole enhancement effect. A tiny droplet of glycerol was dropped on the surface of as-grown SWCNT samples on a quartz substrate, and a series of images were taken during the diffusion process. Three images (a)–(c) are selected from the image series. Between the droplet boundary and the catalyst stripe marked in (b), excess glycerol on the SWCNTs forms microspheres, which dominate the scattering so the SWCNTs do not show chirality-dependent colors. Below the catalyst stripe, the SWCNTs are covered by a wetting layer of glycerol, resulting in interface dipole enhanced Rayleigh scattering of SWCNTs, showing their distinct chirality-dependent colors.

might contribute to the more distinct color. Furthermore, IDEE is not restricted to Rayleigh scattering. Raman and fluorescence signals might also be enhanced by IDEE. The bandgap fluorescence from solutions of SWCNTs wrapped by a surfactant might be also enhanced by interface dipoles. In addition, IDEE can be contributed by a near field of not only interfacial liquid molecules, polymer or surfactant, but also by metal nanoparticles deposited on the surface of the sample provided that the diameters of the metal nanoparticles are smaller than the diameter of CNTs. In this case, the metal nanoparticles serve as interfacial dipoles.

4 Conclusions

We have shown that Rayleigh scattering of SWCNTs can be greatly enhanced by an interfacial layer of condensed molecules. True-color real-time imaging and spectroscopy of SWCNTs for high throughput chirality assignment have been achieved. The enhancement mechanism involved is the local field enhancement due to the local field of interfacial optical dipoles, namely IDEE. As an interface phenomenon, IDEE is negligible for bulk materials, but significant and widespread for nanomaterials surrounded by condensed media. Moreover, we suggest that IDEE might be a more general phenomenon, giving rise to other types of interface dipole enhanced spectroscopy, including not only interface dipole enhanced Rayleigh scattering but also interface dipole enhanced fluorescence and interface dipole enhanced Raman scattering. Lastly, our research indicates that Rayleigh scattering and IDEE might provide a highly effective toolbox for peering into interfacial phenomena.

However, although real-time true-color imaging of nanomaterials has been successfully achieved, the resolution is still limited by optical diffraction, which is not adequate for research in the nanomaterials field. Rayleigh imaging microscopy with super-resolution will be the next important step, calling for further exploration.

5 Methods

5.1 Synthesis and transfer methods of aligned SWCNTs

The SWCNTs were synthesized by CVD on quartz substrates with patterned catalyst stripes of 0.2 nm iron films. Methane was used as the carbon feedstock for the growth of horizontally aligned SWCNTs [18]. PMMA was used as the supporting layer to transfer SWCNTs onto the Si wafer with a layer of 100 nm SiO_2 [19].

5.2 Chirality assignments of SWCNTs based on optical spectra

For SWCNTs which had two resonant peaks between 1.7 and 2.6 eV, the method described in Ref. [7] was adopted for chirality assignments. The optical transition energies of SWCNTs in the atlas in Ref. [20] were red-shifted by 40 meV, as a result of the dielectric screening effect [7]. The chiral indices of SWCNTs were determined by referring to the revised atlas. However, for SWCNTs which had only one resonant peak in the visible range, the additional diameter information from RBM measurements facilitated the chirality assignments.

Acknowledgements

The authors would like to thank Prof. Feng Wang, Prof. Xuedong Bai, and Prof. Kaihui Liu for helpful discussions. This work was supported by the National Basic Research Program of China (No. 2012CB932301) and the National Natural Science Foundation of China (Nos. 90921012, 11321091, 51102144, 11274190, and 51102147).

Electronic Supplementary Material: Supplementary material (a video of the enhanced Rayleigh scattering of SWCNTs on quartz during the glycerol diffusion process) is available free of charge via the Internet at is available in the online version of this article at http://dx.doi.org/10.1007/s12274-015-0779-x.

References

[1] Fabelinskii, I. L. *Molecular Scattering of Light*; Plenum Press: New York, 1968.

[2] Yu, Z.; Brus, L. Rayleigh and Raman scattering from individual carbon nanotube bundles. *J. Phys. Chem. B* **2001**, *105*, 1123–1134.

[3] Sfeir, M. Y.; Wang, F.; Huang, L. M.; Chuang, C. C.; Hone, J.; O'Brien, S. P.; Heinz, T. F.; Brus, L. E. Probing electronic transitions in individual carbon nanotubes by Rayleigh scattering. *Science* **2004**, *306*, 1540–1543.

[4] Berciaud, S.; Voisin, C.; Yan, H.; Chandra, B.; Caldwell, R.; Shan, Y.; Brus, L. E.; Hone, J.; Heinz, T. F. Excitons and high-order optical transitions in individual carbon nanotubes: A Rayleigh scattering spectroscopy study. *Phys. Rev. B* **2010**, *81*, 041414.

[5] Malic, E.; Maultzsch, J.; Reich, S.; Knorr, A. Excitonic Rayleigh scattering spectra of metallic single-walled carbon nanotubes. *Phys. Rev. B* **2010**, *82*, 115439.

[6] Joh, D. Y.; Kinder, J.; Herman, L. H.; Ju, S.; Segal, M. A.; Johnson, J. N.; ChanGarnet, K. L.; Park, J. Single-walled carbon nanotubes as excitonic optical wires. *Nat. Nanotech.* **2011**, *6*, 51–56.

[7] Liu, K. H.; Hong, X. P.; Zhou, Q.; Jin, C. H.; Li, J. H.; Zhou, W. W.; Liu, J.; Wang, E. G.; Zettl, A.; Wang, F. High-throughput optical imaging and spectroscopy of individual carbon nanotubes in devices. *Nat. Nanotech.* **2013**, *8*, 917–922.

[8] Sfeir, M. Y.; Beetz, T.; Wang, F.; Huang, L.; Huang, X. M. H.; Huang, M.; Hone, J.; O'Brien, S.; Misewich, J. A.; Heinz, T. F. et al. Optical spectroscopy of individual single-walled carbon nanotubes of defined chiral structure. *Science* **2006**, *312*, 554–556.

[9] Huang, S.; Qian, Y.; Chen, J.; Cai, Q.; Wan, L.; Wang, S.; Hu, W. Identification of the structures of superlong oriented single-walled carbon nanotube arrays by electrodeposition of metal and Raman spectroscopy. *J. Am. Chem. Soc.* **2008**, *130*, 11860–11861.

[10] Chu, H.; Cui, R.; Wang, J.; Yang, J.; Li, Y. Visualization of individual single-walled carbon nanotubes under an optical microscope as a result of decoration with gold nanoparticles. *Carbon* **2011**, *49*, 1182–1188.

[11] Zhang, R. F.; Zhang, Y. Y.; Zhang, Q.; Xie, H. H.; Wang, H. D.; Nie, J. Q.; Wen, Q.; Wei, F. Optical visualization of individual ultralong carbon nanotubes by chemical vapour deposition of titanium dioxide nanoparticles. *Nat. Commun.* **2013**, *4*, 1727.

[12] Wang, J. T.; Li, T. Y.; Xia, B. Y.; Jin, X.; Wei, H. M.; Wu, W. Y.; Wei, Y.; Wang, J. P.; Liu, P.; Zhang, L. N. et al. Vapor-condensation-assisted optical microscopy for ultralong carbon nanotubes and other nanostructures. *Nano Lett.* **2014**, *14*, 3527–3533.

[13] Klar, T. A.; Jakobs, S.; Dyba, M.; Egner, A.; Hell, S. W. Fluorescence microscopy with diffraction resolution barrier broken by stimulated emission. *P. Natl. Acad. Sci. USA* **2000**, *97*, 8206–8210.

[14] Rust, M. J.; Bates, M.; Zhuang, X. Sub-diffraction-limit imaging by stochastic optical reconstruction microscopy (STORM). *Nat. Methods* **2006**, *3*, 793–796.

[15] Betzig, E.; Patterson, G. H.; Sougrat, R.; Lindwasser, O. W.; Olenych, S.; Bonifacino, J. S.; Davidson, M. W.; Lippincott-Schwartz, J.; Hess, H. F. Imaging intracellular fluorescent proteins at nanometer resolution. *Science* **2006**, *313*, 1642–1645.

[16] Joh, D. Y.; Herman, L. H.; Ju, S. Y.; Kinder, J.; Segal, M. A.; Johnson, J. N.; Chan, G.; Park, J. On-chip Rayleigh imaging

and spectroscopy of carbon nanotubes. *Nano Lett.* **2011**, *11*, 1–7.

[17] Lefebvre, J.; Finnie, P. Polarized light microscopy and spectroscopy of individual single-walled carbon nanotubes. *Nano Res.* **2011**, *4*, 788–794.

[18] Li, J.; He, Y. J.; Han, Y. M.; Liu, K.; Wang, J. P.; Li, Q. Q.; Fan, S. S.; Jiang, K. L. Direct identification of metallic and semiconducting single-walled carbon nanotubes in scanning electron microscopy. *Nano Lett.* **2012**, *12*, 4095-4101.

[19] He, Y. J.; Li, D. Q.; Li, T. Y.; Lin, X. Y.; Zhang, J.; Wei, Y.; Liu, P.; Zhang, L. N.; Wang, J. P.; Li, Q. Q. et al. Metal-film-assisted ultra-clean transfer of single-walled carbon nanotubes. *Nano Res.* **2014**, *7*, 981–989.

[20] Liu, K. H.; Deslippe, J.; Xiao, F. J.; Capaz, R. B.; Hong, X. P.; Aloni, S.; Zettl, A.; Wang, W. L.; Bai, X. D.; Louie, S. G.; Wang, E. G.; Wang, F. An atlas of carbon nanotube optical transitions. *Nat. Nanotech.* **2012**, *7*, 325–329.

[21] Dresselhaus, M. S.; Dresselhaus, G.; Saito, R.; Jorio, A. Raman spectroscopy of carbon nanotubes. *Phys. Rep.* **2005**, *409*, 47–99.

[22] Wang, F.; Sfeir, M. Y.; Huang, L.; Huang, X. H.; Wu, Y.; Kim, J.; Hone, J.; O Brien, S.; Brus, L. E.; Heinz, T. F. Interactions between individual carbon nanotubes studied by Rayleigh scattering spectroscopy. *Phys. Rev. Lett.* **2006**, *96*, 167401.

[23] Liu, K.; Jin, C.; Hong, X.; Kim, J.; Zettl, A.; Wang, E.; Wang, F. Van der Waals-coupled electronic states in incommensurate double-walled carbon nanotubes. *Nature Phys.* **2014**, *10*, 737–742.

[24] Wu, W. Y.; Yue, J. Y.; Li, D. Q.; Lin, X. Y.; Zhu, F. Q.; Yin, X.; Zhu, J.; Dai, X. C.; Liu, P.; Wei, Y. et al. Interface dipole enhancement effect and enhanced Rayleigh scattering. *Nano Res.* **2015**, *8*, 303–319.

[25] Walther, J. H.; Jaffe, R.; Halicioglu, T.; Koumoutsakos, P. Carbon nanotubes in water: Structural characteristics and energetics. *J. Phys. Chem. B* **2001**, *105*, 9980–9987.

[26] Huang, B. D.; Xia, Y. Y.; Zhao, M. W.; Li, F.; Liu, X. D.; Ji, Y. J.; Song, C. Distribution patterns and controllable transport of water inside and outside charged single-walled carbon nanotubes. *J. Chem. Phys.* **2005**, *122*, 0847088.

[27] Feynman, R. P.; Leighton, R. B.; Sands, M. *The Feynman Lectures on Physics, Mainly Electromagnetism and Matter, Volume II;* Addison-Wesley: Reading, Massachusetts, 1977.

[28] Zheng, M.; Jagota, A.; Semke, E. D.; Diner, B. A.; Mclean, R. S.; Lustig, S. R.; Richardson, R. E.; Tassi, N. G. DNA-assisted dispersion and separation of carbon nanotubes. *Nat. Mater.* **2003**, *2*, 338–342.

[29] Arnold, M. S.; Green, A. A.; Hulvat, J. F.; Stupp, S. I.; Hersam, M. C. Sorting carbon nanotubes by electronic structure using density differentiation. *Nat. Nanotech.* **2006**, *1*, 60–65.